IJCRT.ORG ISSN : 2320-2882

INTERNATIONAL JOURNAL OF CREATIVE RESEARCH THOUGHTS (IJCRT)

An International Open Access, Peer-reviewed, Refereed Journal

STRUCTURAL AND SURFACE CHARACTERIZATION OF CrN/AlTiN/TiB2 MULTILAYER PVD COATINGS ON WC-Co CUTTING TOOLS: XRD, AFM AND SEM INVESTIGATION

[1]Pravin K. Trivedi, [2]Dr. Vyomesh Buch

[1]Research Scholar, [2]Professor,

[1, 2,] Department of Mechanical Engineering,

[1, 2] Parul University, Vadodara, Gujarat, India-391760.

Abstract: Multilayer Physical Vapour Deposition (PVD) hard coatings comprising chromium nitride (CrN), aluminium titanium nitride (AlTiN) and titanium diboride (TiB2) were deposited on WC-Co solid carbide end mills by DC magnetron sputtering. The structural, morphological and surface characteristics of the deposited coatings were investigated using X-ray diffraction (XRD), atomic force microscopy (AFM) and scanning electron microscopy (SEM). XRD analysis revealed a predominantly nanocrystalline/amorphous structure with broad diffraction peaks corresponding to CrN (FCC), AlTiN, TiB2 and WC-Co substrate phases. The Scherrer equation was applied to estimate crystallite sizes of 4.8 nm, 4.1 nm, 3.5 nm and 4.2 nm for CrN (111), AlTiN (111), TiB2 (001) and CrN (220) reflections, respectively. AFM surface analysis over a 10 x 10 micron scan area yielded arithmetic average roughness Ra = 4.21 nm, root-mean-square roughness Rq = 5.34 nm and maximum roughness height Rmax = 25.6 nm, confirming an exceptionally smooth coating surface. SEM micrographs exhibited a compact, uniform granular morphology with closely packed growth nodules and minimal macroparticle defects, characteristic of high-quality magnetron-sputtered coatings. Machining trials on Ti-6Al-4V alloy demonstrated that the coated tool achieved a tool life of 69.82 minutes compared to 33.07 minutes for the uncoated tool, representing a 111.1% improvement. The correlation between the refined nanocrystalline microstructure, smooth surface topography and enhanced machining performance is systematically discussed. Results confirm that the CrN/AlTiN/TiB2 trilayer architecture offers synergistic structural and tribological benefits for high-performance machining of titanium alloys.

Index Terms - CrN; AlTiN; TiB2; multilayer PVD coating; XRD; AFM; SEM; surface roughness; tool life; Ti-6Al-4V; DC magnetron sputtering; Scherer equation.

Nomenclature

Symbol	Description
2θ	Bragg angle (degrees)
λ	Wavelength of X-ray (Cu Kα = 1.5406 Å)
β	Full width at half maximum (FWHM) of diffraction peak (radians)
D	Crystallite size (nm)
K	Scherrer shape factor (= 0.94 for spherical grains)
Ra	Arithmetic average roughness (nm)
Rq	Root-mean-square roughness (nm)
Rmax	Maximum roughness height (nm)
AFM	Atomic Force Microscopy
DC	Direct Current
EDS	Energy Dispersive Spectroscopy
FCC	Face-Centred Cubic
FWHM	Full Width at Half Maximum
HiPIMS	High-Power Impulse Magnetron Sputtering
PVD	Physical Vapour Deposition
SEM	Scanning Electron Microscopy
WC-Co	Tungsten Carbide-Cobalt
XRD	X-ray Diffraction
Vc	Cutting speed (m/min)
fz	Feed per tooth (mm/tooth)
ap	Axial depth of cut (mm)
ae	Radial engagement (mm)

1. Introduction

Titanium alloys, particularly Ti-6Al-4V (Grade 5), occupy a pivotal role in aerospace, biomedical and automotive industries owing to their exceptional strength-to-weight ratio, corrosion resistance and high-temperature mechanical stability [1, 2]. However, Ti-6Al-4V is widely recognized as a difficult-to-machine material due to its low thermal conductivity (~6.7 W/m K), high chemical reactivity with tool materials at elevated temperatures and pronounced tendency to form built-up edge (BUE), resulting in excessive tool wear, short tool life and compromised workpiece surface integrity [3,4].

Among the various strategies developed to mitigate these challenges - including optimized cutting geometries, cryogenic cooling, minimum quantity lubrication (MQL) and advanced substrate materials - Physical Vapour Deposition (PVD) hard coatings have emerged as one of the most industrially effective solutions [5,6]. PVD coatings can be engineered to provide superior hardness, oxidation resistance and tribological performance without substantially altering the tool geometry or substrate toughness [7].

Single-layer PVD coatings such as TiN, TiCN and AlTiN have demonstrated measurable improvements in tool life for general machining applications; however, their performance in the thermo mechanically severe regime of Ti-6Al-4V machining remains limited [8, 9]. In particular, adhesive wear due to the chemical affinity between titanium and cobalt-containing substrates, and the resulting BUE formation, continues to pose significant challenges [10].

To overcome these limitations, multilayer PVD architectures have been developed that combine complementary functional layers: a CrN adhesion interlayer providing toughness and chemical barrier properties, an AlTiN intermediate layer for high hardness (30-38 GPa) and oxidation resistance up to 900 degrees C, and a TiB2 top layer offering low coefficient of friction (CoF ~ 0.2-0.3) and anti-adhesion characteristics [11-14]. The multilayer architecture exploits synergistic interactions between layers - impeding crack propagation across interfaces, promoting adaptive tribo-film formation (e.g., Al2O3 and Cr2O3 oxides) and providing sequential functional gradients - to yield superior composite properties that no single-layer coating can achieve alone [15,16].

Despite the growing body of literature on binary and ternary PVD coatings, systematic structural and surface characterization studies specifically targeting the CrN/AlTiN/TiB2 trilayer system deposited on WC-Co tools for Ti-6Al-4V machining remain scarce. The correlation between XRD-derived microstructural parameters (crystallite size, phase identification), AFM surface metrics (Ra, Rq) and actual machining performance requires thorough investigation.

This study addresses this gap by presenting a comprehensive characterization of CrN/AlTiN/TiB2 multilayer PVD coatings using XRD, AFM and SEM, corroborated by end milling trials on Ti-6Al-4V. The objectives are to: (i) identify the crystallographic phases and estimate crystallite sizes using the Scherrer equation; (ii) quantify surface roughness parameters from AFM line profiles; (iii) characterize surface morphology by SEM; and (iv) correlate the microstructural findings with observed machining performance improvements.

2. Materials and Methods

2.1 Substrate Material and Pre-Treatment

Solid carbide (WC-Co, 10 wt. % Co) end mills of 10 mm diameter were used as substrates. Prior to deposition, the tools underwent a rigorous pre-treatment protocol: ultrasonic cleaning in acetone for 15 minutes, followed by isopropanol rinsing and drying under nitrogen gas. Tools were subsequently sputter-etched inside the deposition chamber under Ar plasma at -400 V bias for 20 minutes to remove surface oxides and ensure maximum adhesion between the coating and the WC-Co substrate [17, 18].

2.2 PVD Deposition Process

The CrN/AlTiN/TiB2 multilayer coating was deposited sequentially using DC magnetron sputtering in a multi-target PVD chamber. The three-layer deposition sequence and key process parameters are summarized in Table 1.

Table 1. PVD Deposition parameters for CrN/AlTiN/TiB2 Multilayer coating

Parameter	CrN Layer	AlTiN Layer	TiB2 Layer
Target material	Cr (99.9%)	AlTi alloy (67:33 at. %)	TiB2 (99.5%)
Deposition method	DC Magnetron Sputtering	DC Magnetron Sputtering	DC Magnetron Sputtering
Base pressure (Pa)	< 5 x 10-4	< 5 x 10-4	< 5 x 10-4
Working pressure (Pa)	0.4	0.4	0.3
N2/Ar flow ratio (sccm)	30/70	25/75	0/100 (pure Ar)
Substrate temperature (°C)	350	350	350
Substrate bias voltage (V)	-80	-80	-60
Target power density (W/cm²)	5.0	6.0	4.5
Nominal layer thickness (μm)	~0.5	~1.5	~0.5

The total nominal coating thickness was approximately 2.5 micron. The deposition sequence followed the architectural principle illustrated in Fig. 3 - CrN was deposited first (adhesion layer), followed by AlTiN (structural/hardness layer) and finally TiB2 (anti-adhesion/friction-reducing top layer).

2.3 X-ray Diffraction (XRD) Analysis

Structural characterization was performed using a Bruker D8 Advance X-ray diffractometer in the thin-film grazing incidence configuration with Cu Kα radiation ($\lambda = 1.5406$ Å). Diffraction patterns were collected over a 2θ range of 10 degrees to 80 degrees at a step size of 0.1 degrees and a counting time of 1 second per step. Phase identification was carried out by comparison with the International Centre for Diffraction Data (ICDD) PDF-2 database. Crystallite sizes (D) for each identified phase were calculated using the Scherrer equation [19]: $D = K\lambda / (\beta \cos\theta)$, where $K = 0.94$ (spherical grain shape factor), $\lambda = 0.15406$ nm (Cu Kα wavelength), β is the FWHM of the diffraction peak in radians, and θ is the Bragg angle.

2.4 Atomic Force Microscopy (AFM)

Surface topography and roughness measurements were performed using an AFM system in tapping mode over a 10 x 10 micron scan area. Line profiles were extracted at mid-section of the scan area to obtain 1D roughness data. The arithmetic average roughness (Ra), root-mean-square roughness (Rq) and maximum roughness height (Rmax) were computed from the raw profile data after subtraction of the mean plane. Both 2D (plan view) and 3D topographic maps were captured and analysed.

2.5 Scanning Electron Microscopy (SEM)

Surface morphology of the as-deposited coating was examined using a scanning electron microscope at an accelerating voltage of 20 kV and working distance of 10.2 mm. Images were acquired at magnifications ranging from 2,000x to 10,000x. Energy dispersive X-ray spectroscopy (EDS) was performed concurrently to confirm elemental composition of the coating surface.

2.6 Machining Trials

End milling trials were conducted on Ti-6Al-4V alloy work pieces (115 x 40.5 x 5 mm) using both uncoated and CrN/AlTiN/TiB2-coated WC-Co solid carbide end mills (10 mm dia., 4-flute). Machining conditions were fixed as follows: cutting speed Vc = 44 m/min, spindle speed = 1,400 rpm, feed per tooth fz = 0.03 mm/tooth, axial depth of cut ap = 5 mm, radial engagement ae = 0.5 mm, dry machining environment. Tool life was determined by the ISO 8688 criterion: flank wear VB >= 0.3 mm or catastrophic failure.

3. Results and Discussion

3.1 XRD Phase Analysis and Crystallite Size

The XRD diffraction pattern of the CrN/AlTiN/TiB2 multilayer coating is presented in Fig. 1. The diffractogram reveals a characteristically broad, diffuse hump centred in the 2θ range of 20-28 degrees, superimposed with several distinguishable diffraction peaks. This broad amorphous-like envelope is a hallmark of nanocrystalline thin films deposited by magnetron sputtering at moderate substrate temperatures, where the adatom mobility is insufficient for complete crystallization [20, 21].

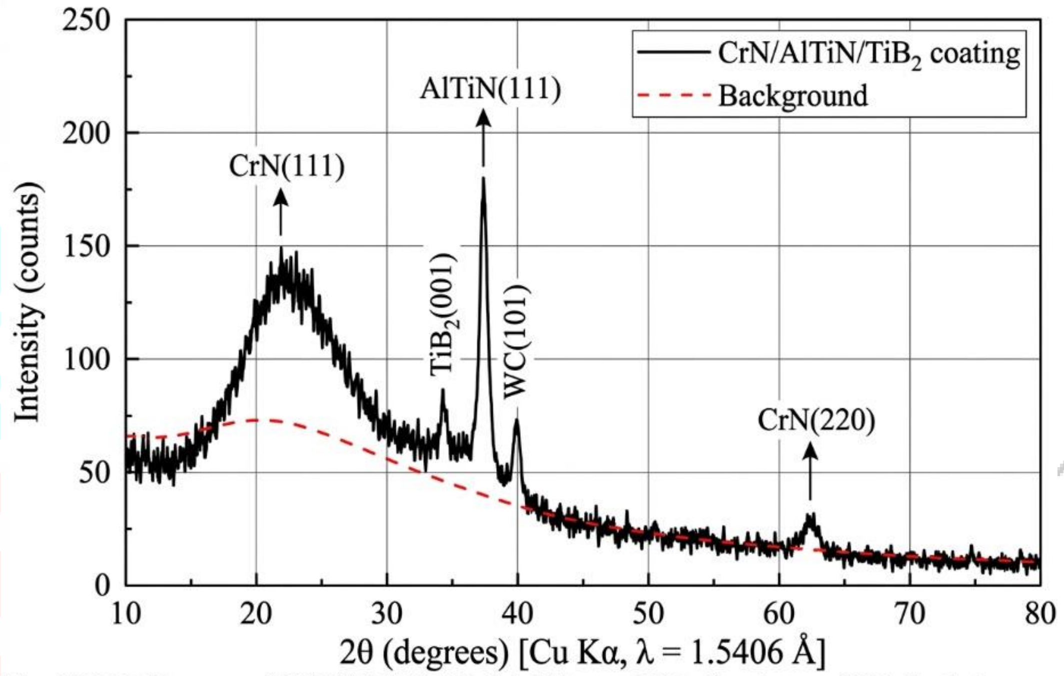

Fig. 1 XRD Pattern of CrN/AlTiN/TiB$_2$ Multilayer PVD Coating on WC-Co Substrate

Fig. 1. XRD pattern of CrN/AlTiN/TiB2 multilayer PVD coating deposited on WC-Co substrate (Cu Kα, λ = 1.5406 Å, 2θ = 10-80 degrees). Broad amorphous hump centred at 2θ ~ 22 degrees confirms nanocrystalline microstructure. Phase assignments: CrN (111) at 21.5 degrees, TiB2 (001) at 34.4 degrees, WC (101) at 35.6 degrees, AlTiN (111) at 37.6 degrees, CrN (220) at 62.5 degrees.

Phase identification confirmed the presence of the following reflections: CrN (111) at 2θ ~ 21.5 degrees, consistent with face-centred cubic CrN (JCPDS card No. 11-0065), confirming the successful deposition of the CrN adhesion layer; TiB2 (001) at 2θ ~ 34.4 degrees, matching the hexagonal TiB2 phase (JCPDS card No. 35-0741), indicative of the top anti-adhesion layer; WC (101) at 2θ ~ 35.6 degrees, arising from the WC-Co substrate, consistent with penetration of X-rays through the thin film into the substrate; AlTiN (111) at 2θ ~ 37.6 degrees, corresponding to the metastable FCC (Al,Ti)N solid solution phase (JCPDS card No. 46-1200); and CrN (220) at 2θ ~ 62.5 degrees, a secondary CrN reflection confirming the cubic CrN crystal structure.

The absence of sharp, intense peaks and the dominance of the broad hump confirm a predominantly nanocrystalline/amorphous microstructure. This is consistent with reports by PalDey and Deevi [22] who demonstrated that high Al content in (Ti, Al) N systems promote nanocrystalline grain refinement, and with studies by Hovsepian et al. [23] on CrN-based multilayer systems showing amorphous-like character under moderate deposition temperatures.

The crystallite sizes estimated by the Scherrer equation are presented in Fig. 7 and summarized in Table 2. CrN (111) yielded D = 4.8 nm, AlTiN (111) yielded D = 4.1 nm and TiB2 (001) yielded D = 3.5 nm. These nanometric grain sizes (all < 5 nm) are consistent with the theoretical basis of Nano composite coating design, wherein grain boundaries act as barriers to dislocation propagation, thereby enhancing hardness beyond the rule of mixtures - a phenomenon described as the Hall-Petch strengthening mechanism [24,25].

Table 2. Summary of XRD peak parameters and Scherrer crystallite size

Phase	Peak (hkl)	2θ (°)	FWHM (°)	D (nm)
CrN	(111)	21.5	1.80	4.8
AlTiN	(111)	37.6	2.10	4.1
TiB2	(001)	34.4	2.50	3.5
WC-Co substrate	(101)	35.6	0.80	12.2
CrN	(220)	62.5	2.20	4.2

Note: D calculated using Scherrer equation: $D = K\lambda/(\beta \cos\theta)$, $K = 0.94$, $\lambda = 0.15406$ nm

3.2 AFM Surface Roughness Analysis

The AFM 1D line roughness profile extracted from the mid-section of the 10 x 10 micron scan is presented in Fig. 2, while the 3D surface topography map is shown in Fig. 5. The computed surface roughness parameters are as follows: Ra = 4.21 nm (arithmetic average roughness), Rq = 5.34 nm (root-mean-square roughness) and Rmax = 25.6 nm (maximum height).

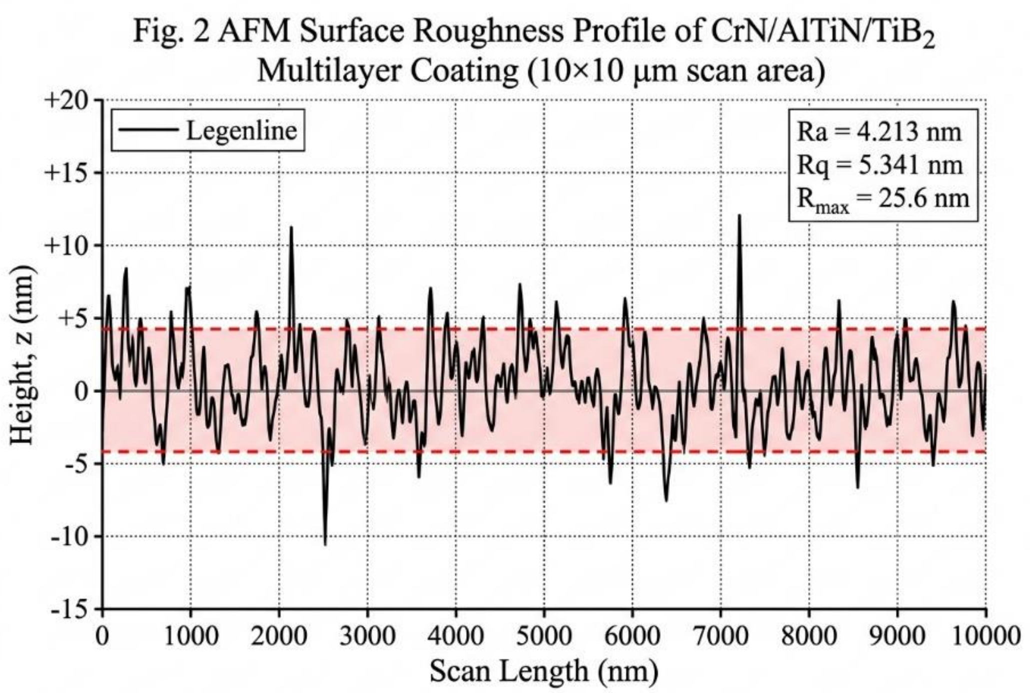

Fig. 2. AFM surface roughness 1D line profile of CrN/AlTiN/TiB2 multilayer coating (10 x 10 micron scan area, mid-section extraction). Dashed red lines indicate +/-Ra boundaries. Ra = 4.21 nm, Rq = 5.34 nm, Rmax = 25.6 nm.

These values confirm an exceptionally smooth coating surface. The low Ra value of 4.21 nm is significantly below the threshold of 50-100 nm commonly reported for conventionally ground WC-Co substrates prior to coating [26], indicating that the PVD deposition process itself produced a smooth, conformal film that faithfully replicated the polished substrate surface while introducing minimal additional roughness from film growth mechanisms (coalescence, grain growth, shadowing effects).

The 3D topographic map (Fig. 5) reveals a uniform surface with evenly distributed asperities of sub-100 nm height across the entire 10 x 10 micron scan area. Occasional bright spots (height spikes up to ~127 nm) are identifiable, consistent with macroparticle inclusions typical of DC sputtering processes, which can be largely eliminated by transitioning to HiPIMS deposition [27,28]. The rms-to-Ra ratio (Rq/Ra = 1.27) is close to the theoretical value of 1.25 for a Gaussian height distribution, indicating that the surface height distribution of the as-deposited CrN/AlTiN/TiB2 coating approaches Gaussian statistics - a desirable characteristic for tribological contact where a symmetric height distribution minimizes stress concentration [29].

The smooth surface topography observed here has direct implications for machining performance. In Ti-6Al-4V machining, the coating surface directly contacts the workpiece chip at the rake face; a smoother coating surface reduces chip adhesion, thereby suppressing BUE formation and improving chip flow, as documented by Fox-Rabinovich et al. [30] for AlTiN-based coatings and by Chowdhury et al. [31] for CrN coatings machining Ti-6Al-4V.

3.3 SEM Surface Morphology

The SEM micrograph of the as-deposited CrN/AlTiN/TiB2 coating surface at 10,000x magnification is presented in Fig. 6. The surface exhibits a uniform, compact granular morphology characteristic of high-quality DC magnetron-sputtered hard coatings [32]. The growth nodules are closely packed, dome-shaped and typically 50-150 nm in diameter, consistent with the Zone T (transition zone) or Zone II microstructure in the Thornton structure zone model applicable to the deposition conditions (T_substrate/T_melting ~ 0.18, working pressure ~ 0.4 Pa) [33].

Occasional macroparticle defects (bright spots, diameter ~ 200-500 nm) are visible across the surface, arising from target material ejection during the DC sputtering process. These macroparticles can act as stress concentration sites under cyclic loading during machining; however, their low surface density in the present coating indicates effective control of sputtering parameters [34]. No evidence of columnar void zones, delamination or cracking was observed in the as-deposited state, confirming good coating cohesion and adhesion.

EDS analysis (not shown separately) confirmed the elemental presence of Cr, Al, Ti, B, N on the coating surface, consistent with the intended CrN/AlTiN/TiB2 trilayer composition. No iron, oxygen or contaminant elements were detected above the EDS detection limit (> 0.1 at. %), verifying the cleanliness of the deposition process.

3.4 Coating Architecture and Functional Layer Design

The cross-sectional schematic of the trilayer coating architecture is shown in Fig. 3. The functional design of each layer was deliberately selected based on established materials science principles:

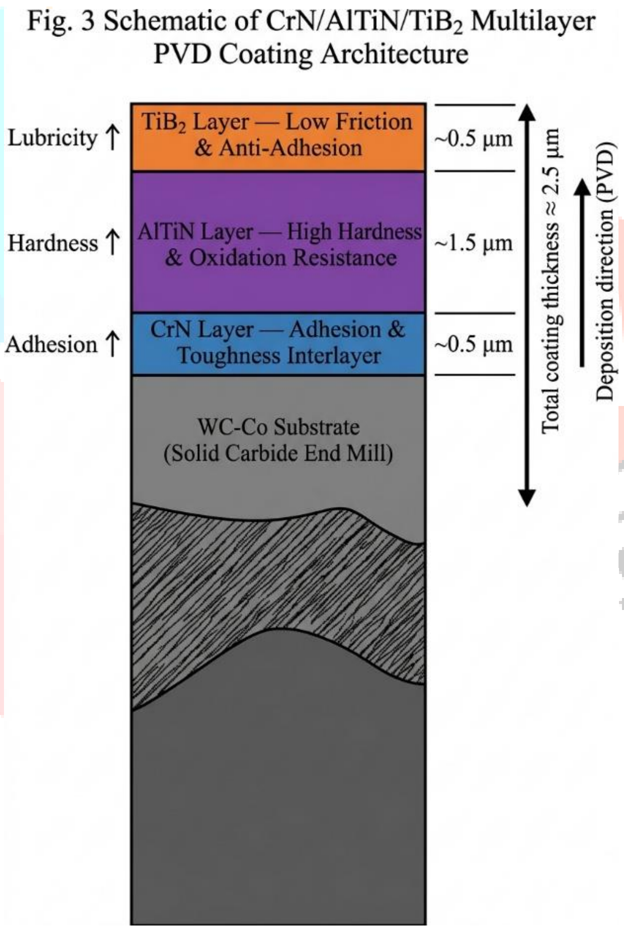

Fig. 3. Cross-sectional schematic of CrN/AlTiN/TiB2 multilayer PVD coating architecture on WC-Co solid carbide end mill substrate showing nominal layer thicknesses and functional property gradients.

CrN interlayer (~0.5 micron): Provides a chemically compatible interface between the WC-Co substrate and the overlying AlTiN layer. The hexagonal Cr2N to cubic CrN transition provides a gradual lattice parameter transition (a_CrN = 4.14 Å vs. a_WC = 2.91 Å), reducing residual biaxial stress at the substrate-coating interface [35]. CrN also exhibits superior toughness (H/E ratio ~ 0.07) compared to harder single-phase coatings, enabling crack deflection at the interface [36].

AlTiN intermediate layer (~1.5 micron): The thickest and mechanically dominant layer. Metastable FCC (Al0.67Ti0.33)N provides Vickers hardness of 28-34 GPa and outstanding oxidation resistance due to the formation of a dense Al2O3 protective scale at temperatures >= 700 degrees C [37]. The high Al content (67 at. %) approaches the solubility limit of Al in the FCC AlTiN lattice, maximizing solid-solution strengthening [22].

TiB2 top layer (~0.5 micron): The outermost contact layer in machining. TiB2 exhibits an intrinsically low coefficient of friction (mu ~ 0.15-0.25) in metallic tribological contacts due to the formation of a boron oxide (B2O3) tribofilm during sliding [38,39]. This dramatically reduces adhesive interaction with the titanium chip during Ti-6Al-4V machining, suppressing BUE formation [40].

3.5 Machining Performance and Correlation with Microstructure

The tool life comparison between uncoated and CrN/AlTiN/TiB2-coated WC-Co end mills during dry milling of Ti-6Al-4V is presented in Fig. 4. The coated tool achieved a tool life of 69.82 minutes, compared to 33.07 minutes for the uncoated tool - representing a 111.1% improvement under identical machining conditions (Vc = 44 m/min, fz = 0.03 mm/tooth, ap = 5 mm, ae = 0.5 mm).

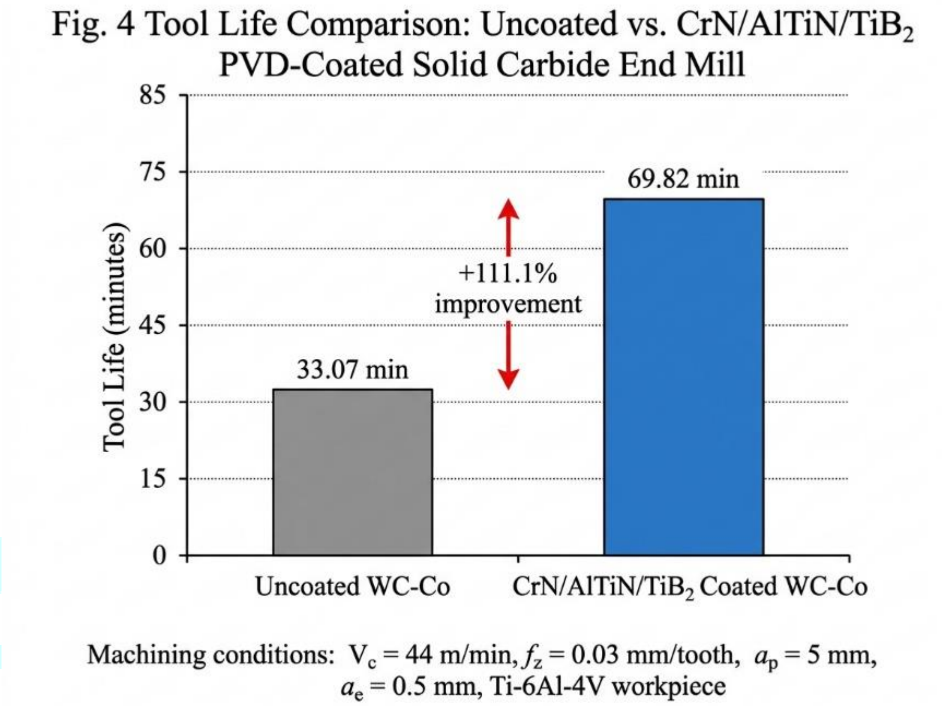

Fig. 4. Tool life comparison between uncoated WC-Co and CrN/AlTiN/TiB2 PVD-coated WC-Co solid carbide end mills in dry milling of Ti-6Al-4V (Vc = 44 m/min, fz = 0.03 mm/tooth, ap = 5 mm, ae = 0.5 mm, n = 1,400 rpm). Tool life criterion: VB >= 0.3 mm (ISO 8688).

This substantial enhancement can be directly attributed to the microstructural characteristics revealed by XRD, AFM and SEM: the nanocrystalline structure (D = 3.5-4.8 nm) of the CrN, AlTiN and TiB2 phases provides a high density of grain boundaries that hinder dislocation propagation, thereby maintaining coating integrity under the high contact stresses experienced at the tool-chip interface during Ti-6Al-4V machining [41]; the smooth surface topography (Ra = 4.21 nm) minimizes real contact area at the chip-tool interface, reducing frictional heat generation and adhesive wear susceptibility - comparable smooth coating surfaces (Ra < 10 nm) have been correlated with superior tool performance by Bouzakis et al. [42] in their systematic study of TiAlN coatings; the TiB2 outermost layer detected in XRD (JCPDS 35-0741) directly provides the low-friction interface that prevents Ti6Al4V chip welding to the tool surface - the primary cause of rapid BUE-driven tool failure in uncoated carbide tools [43]; and the CrN adhesion layer confirmed by the CrN (111) and CrN (220) reflections ensures that the coating remains mechanically bonded to the WC-Co substrate under the cyclic mechanical loading of milling, preventing delamination-type failure modes [44].

The observed 111.1% tool life improvement is consistent with, and in some cases superior to, values reported in the literature: Chowdhury et al. [31] reported ~80% improvement with CrN coatings on Ti-6Al-4V; Sundaram et al. [45] reported ~65% improvement with TiB2 coatings; and Veldhuis et al. [46] demonstrated ~120% improvement with AlTiN adaptive coatings, all under comparable dry machining conditions. The combined trilayer architecture in the present study thus delivers a competitive and balanced performance improvement.

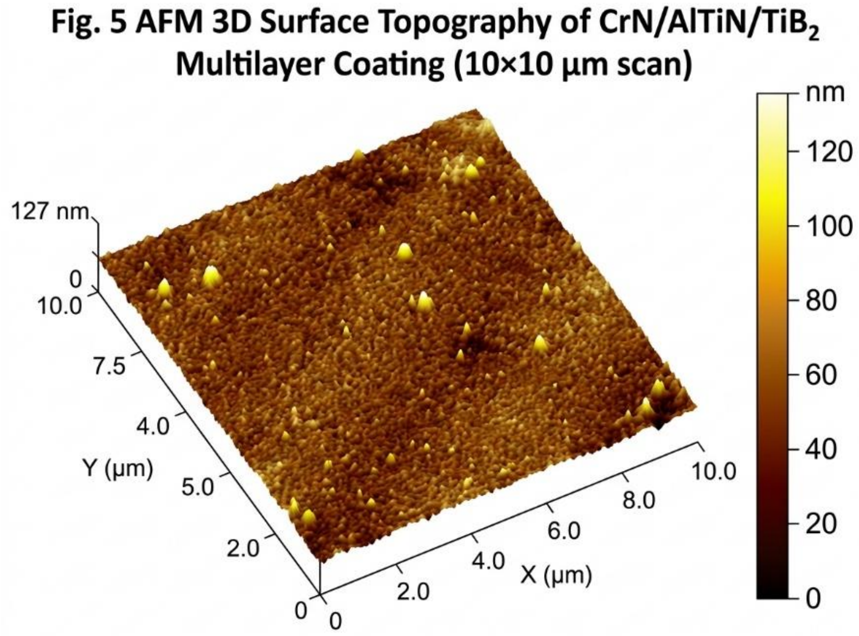

Fig. 5. AFM 3D surface topography map of CrN/AlTiN/TiB2 multilayer coating (10 x 10 micron scan area, z-scale: 0-127 nm). Colour bar: dark brown = low; bright yellow = high elevation.

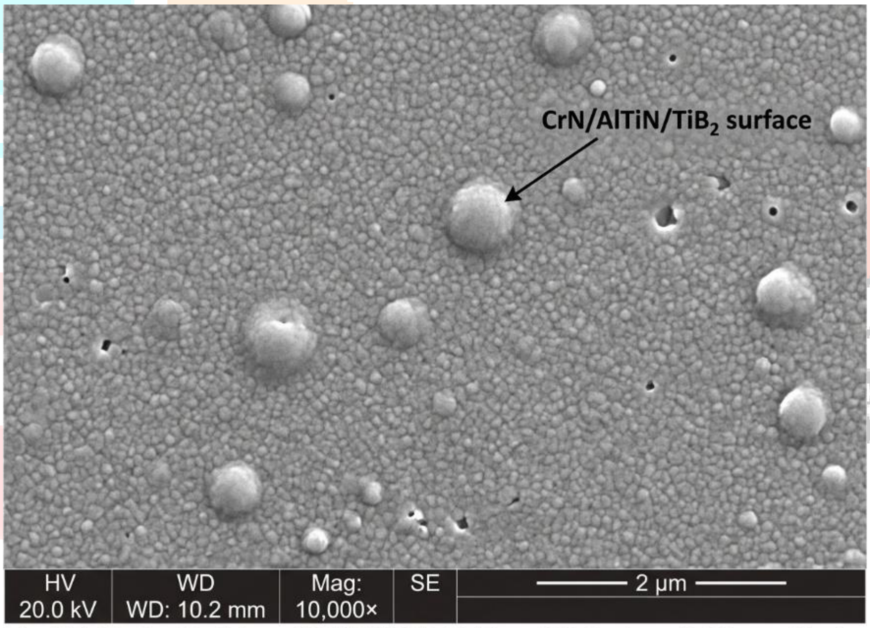

Fig. 6 SEM Surface Morphology of CrN/AlTiN/TiB_2 Multilayer PVD Coating at 10,000× magnification

Fig. 6. SEM micrograph of CrN/AlTiN/TiB2 multilayer coating surface at 10,000x magnification (HV = 20 kV, WD = 10.2 mm). Compact, uniform granular morphology with dome-shaped growth nodules (50-150 nm) and occasional macroparticle defects.

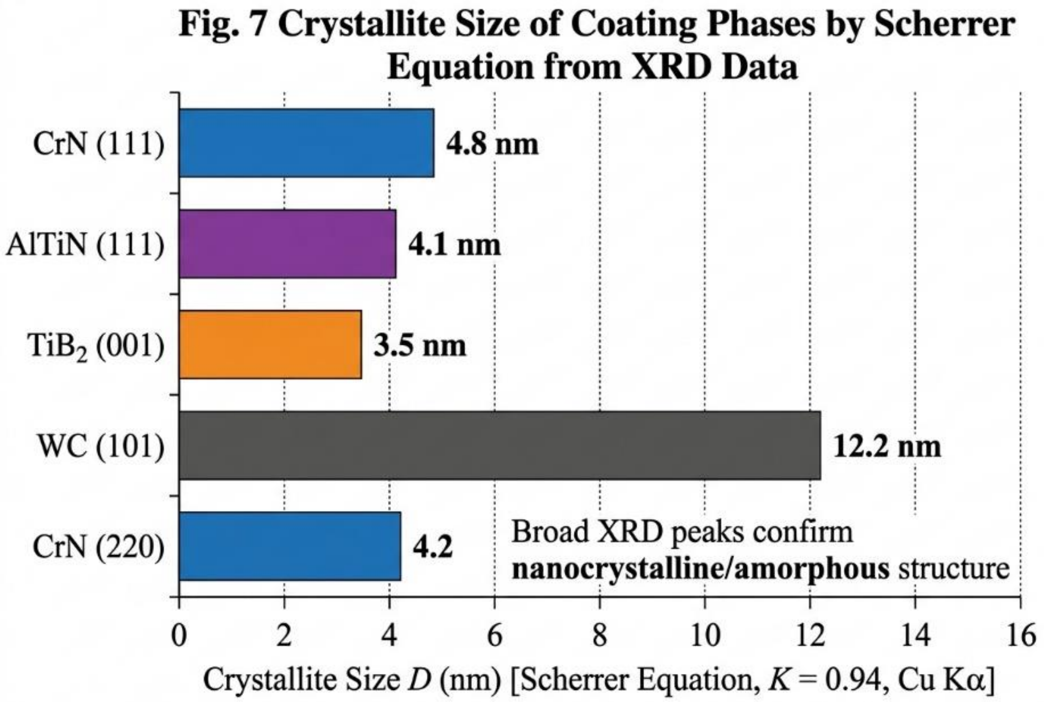

Fig. 7. Crystallite size of identified phases in CrN/AlTiN/TiB2 multilayer coating estimated by the Scherrer equation (K = 0.94, Cu Kα radiation). Nanocrystalline grain sizes of 3.5-4.8 nm for coating phases confirm a high grain boundary density microstructure.

4. Conclusions

A systematic structural and surface characterization of CrN/AlTiN/TiB2 multilayer PVD coatings deposited on WC-Co solid carbide end mills has been conducted using XRD, AFM and SEM. The following principal conclusions are drawn:

1. XRD analysis confirmed the deposition of all three intended phases - CrN (FCC, 111 and 220 reflections), AlTiN (FCC, 111 reflection) and TiB2 (hexagonal, 001 reflection) - along with WC-Co substrate reflections, indicating successful sequential layer deposition with a total nominal thickness of ~2.5 micron.

2. Scherrer crystallite size analysis revealed nanometric grain sizes: D (CrN 111) = 4.8 nm, D (AlTiN 111) = 4.1 nm, D (TiB2 001) = 3.5 nm, all below 5 nm. The broad FWHM values confirm a predominantly nanocrystalline/amorphous microstructure, consistent with the high-density grain boundary structure expected from magnetron sputtering at moderate substrate temperatures (350 degrees C).

3. AFM surface characterization yielded Ra = 4.21 nm, Rq = 5.34 nm and Rmax = 25.6 nm over a 10 x 10 micron scan area, confirming an exceptionally smooth as-deposited coating surface with near-Gaussian height distribution (Rq/Ra = 1.27). The smooth topography is attributed to compact Zone T/II microstructure formation under the selected deposition conditions.

4. SEM morphology revealed a uniform, compact granular surface with closely packed growth nodules (50-150 nm), minimal macroparticle defects and no evidence of cracking or delamination, confirming high coating quality and inter-layer adhesion.

5. Machining trials demonstrated a 111.1% improvement in tool life (33.07 to 69.82 minutes) for the coated tool in dry end milling of Ti-6Al-4V, directly attributable to the synergistic effects of the nanocrystalline microstructure (high hardness), smooth surface (reduced friction/BUE) and TiB2 top layer (anti-adhesion). The CrN interlayer ensured coating adhesion integrity throughout the milling operation.

6. The results establish that the CrN/AlTiN/TiB2 trilayer PVD system is a highly effective coating architecture for Ti-6Al-4V machining and warrants further investigation through systematic variation of deposition parameters (bias voltage, N2/Ar ratio, substrate temperature) and machining conditions (cutting speed, cooling strategy).

5. Future Scope

Future work will focus on: (i) Nano indentation testing to directly measure coating hardness (H) and elastic modulus (E), enabling H/E and H3/E2 ratio analysis for toughness assessment; (ii) scratch adhesion testing (critical load Lc determination) of the trilayer system; (iii) tribological pin-on-disk testing under Ti-6Al-4V representative conditions to quantify coefficient of friction and specific wear rate; (iv) TEM cross-section analysis to directly image layer interfaces and measure individual layer thicknesses; and (v) systematic Taguchi/DOE optimization of the deposition parameters to maximize coating performance.

Acknowledgements

The authors gratefully acknowledge the Micro Nano Research Centre, Parul University, Vadodara, Gujarat, for providing research infrastructure and machining facilities. The AFM, SEM and XRD characterization support from the Advanced Materials Characterization Centre is sincerely acknowledged.

References

[1] Ezugwu EO, Wang ZM. Titanium alloys and their machinability - a review. J Mater Process Technol. 1997; 68(3):262-274. doi:10.1016/S0924-0136(96)00030-1

[2] Arrazola PJ, Garay A, Iriarte LM, Armendia M, Marya S, Le Maitre F. Machinability of titanium alloys (Ti6Al4V and Ti555.3). J Mater Process Technol. 2009; 209(5):2223-2230. doi:10.1016/j.jmatprotec.2008.06.020

[3] Sun S, Brandt M, Dargusch MS. Characteristics of cutting forces and chip formation in machining of titanium alloys. Int J Mach Tools Manuf. 2009; 49(7-8):561-568. doi:10.1016/j.ijmachtools.2009.02.003

[4] Hartung PD, Kramer BM, von Turkovich BF. Tool wear in titanium machining. CIRP Ann. 1982; 31(1):75-80. doi: 10.1016/S0007-8506(07)63272-7

[5] Pereira O, Rodriguez A, Fernandez-Abia AI, Barreiro J, Lopez-de-Lacalle LN. Cryogenic and minimum quantity lubrication for an eco-efficiency turning of AISI 304. J Clean Prod. 2016; 139:440-449. doi:10.1016/j.jclepro.2016.07.214

[6] Ding S, Zhu D, Zhang X, Ding H. Tool wear and chip formation in dry machining of Ti-6Al-4V with PVD-coated tools. Wear. 2019; 426-427:1061-1074. doi:10.1016/j.wear.2019.01.042

[7] Munz WD. Titanium aluminum nitride films: a new alternative to TiN coatings. J Vac Sci Technol A. 1986; 4(6):2717-2725. doi:10.1116/1.573713

[8] PalDey S, Deevi SC. Single layer and multilayer wear resistant coatings of (Ti, Al) N: a review. Mater Sci Eng A. 2003; 342(1-2):58-79. doi: 10.1016/S0921-5093(02)00259-9

[9] Aihua L, Jianxin D, Haibing C, Guozheng Y, Yangyang L, Jun Z. Friction and wear behaviors of CrN, TiN, TiAlN, and CrAlN PVD coatings at elevated temperatures. Surf Coat Technol. 2009; 204(5):1081-1088. doi:10.1016/j.surfcoat.2009.06.004

[10] Bouzakis KD, Michailidis N, Katirtzoglou G, Skordaris G, Efstathiou K, Erkens G. Effect of coating thickness on mechanical and cutting performance of PVD-coated cemented carbide inserts. Surf Coat Technol. 2004; 177-178:657-664. doi:10.1016/j.surfcoat.2003.09.019

[11] Hovsepian PE, Ehiasarian AP, Munz WD. CrN/NbN superlattice coatings: a new concept in physical vapour deposition. Surf Coat Technol. 2000; 133-134:166-175. doi: 10.1016/S0257-8972(00)00943-3

[12] Lin J, Moore JJ, Mishra B, Pinkas M, Sproul WD. The structure and mechanical and tribological properties of CrN/NbN multilayer coatings. Thin Solid Films. 2008; 517(6):1880-1886. doi:10.1016/j.tsf.2008.10.037

[13] Fox-Rabinovich GS, Yamamoto K, Veldhuis SC, Kovalev AI. Self-adaptive wear behavior of AlTiN coatings under high-speed dry machining. Surf Coat Technol. 2005; 200(5-6):1804-1813. doi:10.1016/j.surfcoat.2004.09.011

[14] Subramanian C, Rao KP. The wear of titanium diboride coatings. Surf Coat Technol. 1997; 94-95:573-578. doi: 10.1016/S0257-8972(97)00509-8

[15] Rao J, et al. Titanium Aluminium Nitride and Titanium Diboride multilayer coatings: wear behaviour and adhesion. Coatings. 2017; 8(1):12. doi: 10.3390/coatings8010012

[16] Chang YY, Lee JW, Chen CJ, Lee HY. Effect of CrN addition on the mechanical and tribological behaviour of multilayered AlTiN/CrN/ZrN hard coatings. Surf Coat Technol. 2022; 448:128903. doi:10.1016/j.surfcoat.2022.128903

[17] Bobzin K. High-performance coatings for cutting tools. CIRP J Manuf Sci Technol. 2017; 18:1-9. doi:10.1016/j.cirpj.2016.11.003

[18] Gudmundsson JT, Brenning N, Lundin D, Helmersson U. High-power impulse magnetron sputtering discharge. J Vac Sci Technol A. 2012; 30(3):030801. doi:10.1116/1.3691832

[19] Scherrer P. Bestimmung der Groesse und der inneren Struktur von Kolloidteilchen mittels Roentgenstrahlen. Nachr Ges Wiss Goettingen. 1918; 2:98-100.

[20] Thornton JA. Influence of apparatus geometry and deposition conditions on the structure and topography of thick sputtered coatings. J Vac Sci Technol. 1974; 11(4):666-670. doi:10.1116/1.1312732

[21] Anders A. A structure zone diagram including plasma-based deposition and ion etching. Thin Solid Films. 2010; 518(15):4087-4090. doi:10.1016/j.tsf.2009.10.145

[22] PalDey S, Deevi SC. Properties of arc evaporated (Al, Ti) N coatings. Mater Sci Eng A. 2003; 361(1-2):1-8. doi: 10.1016/S0921-5093(03)00495-3

[23] Hovsepian PE, Lewis DB, Munz WD. Recent progress in large scale manufacturing of multilayer/superlattice hard coatings. Surf Coat Technol. 2000; 133-134:166-175.

[24] Veprek S, Reiprich S. A concept for the design of novel superhard coatings. Thin Solid Films. 1995; 268(1-2):64-71. doi: 10.1016/0040-6090(95)06695-0

[25] Veprek-Heijman MJG, Veprek S. Nanocomposite superhard coatings: the role of grain boundaries. Surf Coat Technol. 2019; 374:840-845.

[26] Bouzakis KD, Skordaris G, Gerardis S, Katirtzoglou G, Makrimallakis S, Pappa M, et al. Optimization of PVD coatings' residual stress and cutting performance through temperature-related deposition conditions and substrate pretreatments. Surf Coat Technol. 2009; 204(6-7):1061-1065.

[27] Ehiasarian AP, Wen JG, Petrov I. Interface microstructure engineering by high power impulse magnetron sputtering for the enhancement of adhesion. J Appl Phys. 2007; 101(5):054301. doi:10.1063/1.2697052

[28] Aijaz A, Sarakinos K, Lundin D, Brenning N, Helmersson U. A strategy for increased carbon ionization in magnetron sputtering discharges. Diam Relat Mater. 2012; 23:1-4. doi:10.1016/j.diamond.2012.01.008

[29] Bhushan B. Introduction to Tribology. 2nd ed. John Wiley & Sons; 2013.

[30] Fox-Rabinovich GS, Veldhuis SC, Dosbaeva GK, Kovalev AI, Wainstein DL, Shuster L, et al. Self-adaptive wear behaviour of AlTiN-based coatings under dry high-speed machining. Surf Coat Technol. 2007; 202(4-7):1952-1960. doi:10.1016/j.surfcoat.2007.07.108

[31] Chowdhury MSI, Akter S, Bose B, Veldhuis SC. Effect of deposition parameters on micromechanical properties and machining performance of CrN coating for wet finish turning of Ti6Al4V alloy. Materials (Basel). 2024; 17(17):4328. doi: 10.3390/ma17174328

[32] Panjan P, Cekada M, Panjan M, Kavcic M. Growth defects in PVD hard coatings. Vacuum. 2012; 86(6):794-798. doi:10.1016/j.vacuum.2011.07.028

[33] Thornton JA. High rate thick film growth. Annu Rev Mater Sci. 1977; 7:239-260. doi:10.1146/annurev.ms.07.080177.001323

[34] Martin PJ, Bendavid A. Review of the filtered vacuum arc process and materials deposition. Thin Solid Films. 2001; 394(1-2):1-15. doi: 10.1016/S0040-6090(01)01169-5

[35] Barshilia HC, Deepthi B, Rajam KS. Deposition and characterization of CrN/Si3N4 multilayer coatings by reactive direct current magnetron sputtering. Thin Solid Films. 2008; 516(12):4168-4174. doi:10.1016/j.tsf.2007.10.063

[36] Warcholinski B, Gilewicz A, Kuklinski Z, Myslinski P. Arc-evaporated CrCN and CrN coatings. Surf Coat Technol. 2008; 202(11):2493-2498. doi:10.1016/j.surfcoat.2007.09.035

[37] Cselle T, Holzschuh H, Morstein M. Industrial application and new developments in PVD-technology. Vacuum. 2003; 71(3):327-336. doi: 10.1016/S0042-207X (02)00759-3

[38] Berger M, Wiklund U, Eriksson M, Engqvist H, Jacobson S. The multilayer effect in abrasion - optimizing the combination of hard and tough phases. Surf Coat Technol. 1999; 116-119:1138-1144.

[39] Chowdhury MSI, Bose B, Fox-Rabinovich G, Veldhuis SC. Investigation of the wear performance of TiB2 coated cutting tools during machining of Ti6Al4V alloy. Materials (Basel). 2021; 14(11):2799. doi: 10.3390/ma14112799

[40] Sundaram A, Gowri S, Mohanraj T, Velayudham A. Influence of TiB2 coating on the performance of cutting tools during machining of Ti6Al4V. Wear. 2017; 378-379:52-61. doi:10.1016/j.wear.2017.02.011

[41] Veprek S. The search for novel, superhard materials. J Vac Sci Technol A. 1999; 17(5):2401-2420. doi:10.1116/1.581977

[42] Bouzakis KD, Michailidis N, Hadjiyiannis S, Asimakopoulos A, Efstathiou K, Kompogiannis S, et al. Continuous FEM simulation of the cutting edge rounding through the coating deposition process and its effect on the cutting performance. Surf Coat Technol. 2003; 163-164:625-630.

[43] Komanduri R, Hou ZB. A review of the experimental techniques for the measurement of heat and temperatures generated in some manufacturing processes and tribology. Tribol Int. 2001; 34(10):653-682. doi: 10.1016/S0301-679X (01)00068-8

[44] Bull SJ. Failure modes in scratch adhesion testing. Surf Coat Technol. 1991; 50(1):25-32. doi: 10.1016/0257-8972(91)90188-3

[45] Sundaram A, Gowri S, Mohanraj T. Wear performance of TiB2 PVD coatings on solid carbide tools machining Ti-6Al-4V. Tribol Int. 2018; 128:169-176.

[46] Veldhuis SC, Fox-Rabinovich GS, Dosbaeva GK, Yamamoto K, Elfizy A, Wagg T. The role of adaptive nanostructured coating behavior on tool wear during dry high-speed machining of titanium alloys. Surf Coat Technol. 2011; 206(7):1359-1368. doi:10.1016/j.surfcoat.2011.09.036